Cholesterol constrains the antigenic configuration of the membrane-proximal neutralizing HIV-1 epitope

Johana Torralba[1,2], Igor de la Arada[1], Pablo Carravilla[1,2,3,4], Sara Insausti[1,2], Edurne Rujas[1,2], Eneko Largo[1,5], Christian Eggeling[3,4,6], José L. R. Arrondo[1,2], Beatriz Apellániz[1,7*] and José L. Nieva[1,2*]

[1]Biofisika Institute (CSIC, UPV/EHU), University of the Basque Country (UPV/EHU), PO Box 644, 48080 Bilbao, Spain.

[2]Department of Biochemistry and Molecular Biology, University of the Basque Country (UPV/EHU), PO Box 644, 48080 Bilbao, Spain.

[3]Institute of Applied Optics and Biophysics Friedrich-Schiller-University Jena, Max-Wien Platz 1, 07743 Jena, Germany.

[4]Leibniz Institute of Photonic Technology e.V., Albert-Einstein-Straße 9, 07745 Jena, Germany.

[5]Department of Immunology, Microbiology and Parasitology, Medicine and Odontology Faculty, University of Basque Country (UPV/EHU), PO Box 644, 48080 Bilbao, Spain.

[6]MRC Human Immunology Unit, Weatherall Institute of Molecular Medicine, University of Oxford, Headley Way, OX3 9DS Oxford, UK.

[7]Department of Physiology, Faculty of Pharmacy, University of the Basque Country (UPV/EHU), Paseo de la Universidad, 7, 01006 Vitoria-Gasteiz, Spain.

*Correspondence to: beatriz.apellaniz@ehu.eus; joseluis.nieva@ehu.es

The envelope glycoprotein (Env) enables HIV-1 cell entry through fusion of host-cell and viral membranes induced by the transmembrane subunit gp41. Antibodies targeting the C-terminal sequence of the Membrane-Proximal External Region (C-MPER) block the fusogenic activity of gp41 and achieve neutralization of divergent HIV-1 strains and isolates. Thus, recreating the structure that generates broadly neutralizing C-MPER antibodies during infection is a major goal in HIV vaccine development. Here, we have reconstituted a peptide termed CpreTM-TMD in a membrane environment. This peptide contains the C-MPER epitope and the minimum TMD residues required for the anchorage of the Env glycoprotein to the viral membrane. In addition, we have used antibody 10E8 variants to gauge the antigenic configuration attained by CpreTM-TMD as a function of the membrane cholesterol content, a functional determinant of the HIV envelope and liposome-based vaccines. Differential binding of the 10E8 variants and the trend of the IgG responses recovered from rabbits immunized with liposome-peptide formulations, suggested that cholesterol may restrict 10E8 accessibility to the C-MPER epitope. Our data ruled out the destabilization of the lipid bilayer architecture in CpreTM-TMD-containing membranes, and pointed to the perturbation of the helical conformation by lipid packing as the cause of the antigenic configuration loss induced by cholesterol. Overall, our results provide additional insights into the structural basis of the Env complex anchoring to membranes, and suggest new approaches to the design of effective immunogens directed against the near pan-neutralizing HIV-1 epitope C-MPER.

Keywords: HIV-1 MPER; HIV-1 TMD; neutralizing antibody 10E8; MPER vaccine; membrane cholesterol; lipid packing

Fusion with the target host-cell membrane marks the beginning of the Human Immunodeficiency Virus type-1 (HIV-1) replication cycle [1-4]. The transmembrane subunit gp41 of the envelope glycoprotein (Env) promotes the process by the concerted action of two types of structural elements: i) two highly conserved membrane-inserting regions, one at the free N-terminus and the other proximal to the viral membrane [5]; and ii) helical domains or heptad repeats (HRs) that refold forming an energetically favorable, trimeric 6-helix bundle [6]. The membrane-inserting sequence at the N-terminus constitutes the fusion peptide (FP) (reviewed in [5]). After fusion triggering by receptor (CD4)/co-receptor engagement (CXCR4 or CCR5), the FP is propelled towards de cell membrane and embeds therein due to its hydrophobic character [2-4]. However, the tip of the FP remains exposed to the solvent in one of the conformational states of the pre-fusion Env complex [7-8], and is accessible to antibodies that neutralize HIV-1 with modest potency and breadth [9-10].

The sequence inserting into the viral membrane, also known as the Membrane-Proximal External Region (MPER), is exceptionally enriched in aromatic residues that promote interactions with the membrane interface [11-14]. Structural analyses suggest that the C-terminal residues of MPER (C-MPER, Env residues 671-683, HXB2 numbering) can combine with N-terminal residues of the transmembrane domain (TMD, Env residues 684-690) into a single continuous helix [15-21]. CpreTM, a peptide spanning this region can induce lipid bilayer restructuring upon partitioning into cholesterol (Chol)-enriched virus-like membranes [22-24]. Thus, the membrane activity of this sequence, unleashed after fusion activation, is postulated to help the fusion process proceed by perturbing the highly rigid HIV lipid envelope [25] (Fig S1a).

Importantly, the conserved C-MPER sequence is immunogenic during infection [26-28], which underscores the existence of a structurally stable state of this Env region

accessible to B-cell receptors, at least within one of the conformational states visited by the pre-fusion complex [29-30]. Further supporting the existence of a structurally defined C-MPER epitope common to diverse pre-fusion Env variants, all anti-C-MPER broadly neutralizing antibodies (bnAbs) that have been isolated so far (e.g, 4E10, 10E8 or LN01), recognize the same surface of the C-MPER helix, and consistently display the broadest coverage among the HIV-1 bnAb classes [21, 26-27, 31-34]. Using super-resolution microscopy we have recently demonstrated that C-MPER is indeed accessible to the bnAbs 4E10 and 10E8 on the surface of intact virions [35].

Atomic structure resolution of bnAbs 4E10, 10E8 and LN01 in complex with lipids [21, 36-37], or with epitope-peptides elongated to include TMD residues [19, 21], in combination with cryo-electron microscopy (cryo-EM) reconstructions of Env-Fab complexes [17, 34], has provided a model for the molecular recognition of C-MPER at the virus membrane surface (Figure 1). According to this model, monomers of continuous helices spanning the MPER-TMD region stick out the membrane with similar topologies, with angles ranging from slightly tilted to almost perpendicular to the membrane plane, and antibodies nonspecifically adsorbed to the interfacial region of the membrane approach the C-MPER epitope laterally. However, in analogy with the dynamic conformation of the pre-fusion Env ectodomain [7-8, 29-30], cumulative evidence supports the conformational pliability of MPER-TMD helices, which, depending on the sequence range considered, membrane dose and lipid composition, may adopt in the unbound conformation membrane structures differing in oligomeric state, insertion angle or C-MPER epitope exposure [13-15, 18, 20, 38-39]. Interestingly, recent studies report a transmembrane helix tilt angle of ca. 45º for a TMD peptide elongated at its C-terminus [20] or the total occlusion of C-MPER antigenic face into the membrane when a peptide is elongated to contain the full MPER sequence at its N-terminus [13]. Thus, the membrane-

inserted states adopted by these peptides appear to be incompatible with the proposed mechanism of lateral Env docking of anti-C-MPER antibodies [17, 19, 36-37].

In an attempt to mimic the membrane-inserted MPER structure that elicits anti-C-MPER antibodies, in this study we have addressed the reconstitution of the C-MPER epitope recognized by bnAb 10E8 in liposome vaccines. To that end, we employ peptides that combine the C-MPER epitope with the minimal TMD anchor of Env previously described by Yue et al. [40] In addition, we have generated bnAb 10E8 mutants that can be used as reference standards to measure the antigenicity profile of the reconstituted peptides. We demonstrate that the C-MPER epitope can attain a correct configuration in membranes, but that high concentration of Chol induces its concealment. We propose a model that, besides providing new insights into the molecular basis of Env-anchoring to the viral membrane, may inform the design of immunogenic formulations aimed at boosting anti-C-MPER bnAb production.

RESULTS

Design of a C-MPER epitope peptide with a membrane anchor

The model in Figure 1a reflects the capacity of the native Env trimer for sampling different conformational states [30], with the C-MPER epitope becoming accessible to the bnAb 10E8 within one of such states [35]. Panel 1b displays a detailed view of 10E8 docking to Env in the pre-fusion state [17, 19, 37]. From this model one can infer that 10E8 binding to Env would freeze the CpreTM region in an upright position, preventing further interaction with the viral membrane and, hence, fusion to proceed (Figure S1a). Panel 1b highlights the three elements of the Fab 10E8 involved in the efficient engagement with the C-MPER epitope at membranes, namely, (1) the specificity binding pocket, (2) an accommodation surface with the membrane interface, and (3) an area in contact with the Env complex ectodomain [19, 26, 37].

As explained in the diagrams depicted in Figures 1c and S1b, in this study we seek to reproduce the components (1) and (2) of the interaction by reconstituting in liposome vaccines the peptide CpreTM-TMD (Env residues 671-700, HXB2 numbering). This peptide encompasses the full 10E8 epitope and a minimal membrane anchor of Env [40]. In addition, it contains Lys-tags to increase solubility at both ends of the molecule [16]. In contrast to the shorter CpreTM peptide that destabilizes the membrane architecture [22, 24-25], or longer peptides that seem to conceal the C-MPER epitope [13, 20, 38], we expected the CpreTM-TMD peptide to span the lipid bilayer without affecting its integrity, and to expose the antigenic face of the C-MPER helix accessible for its engagement with antibodies and B-cell receptors (Figure 1c, right). Thus, in our approach we reasoned that a scaffold peptide with a minimal TMD would force the upright orientation of the

helix and ensure at the same time an efficient exposure of the C-MPER epitope at the membrane interface (Figure S1b).

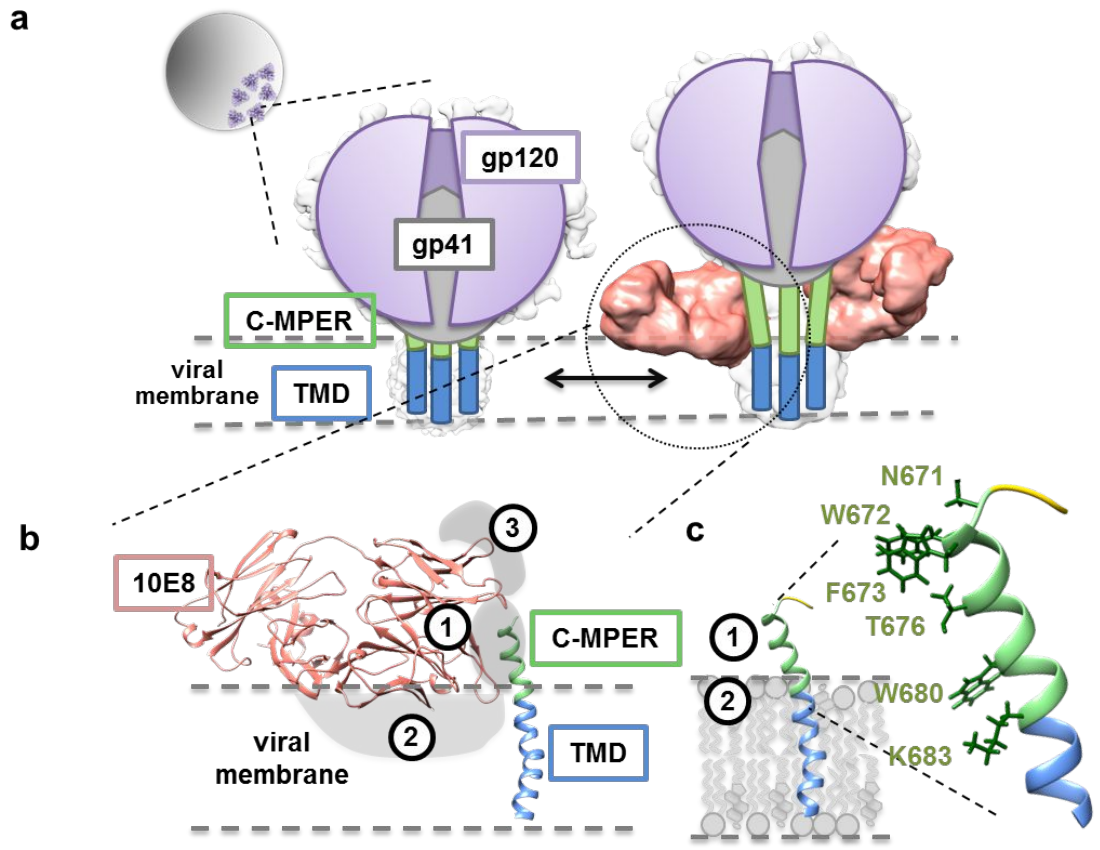

Figure 1: Schematics depicting the accessibility of the HIV-1 neutralizing epitope MPER at the viral membrane interface. (a) Model for accessibility of the C-terminal section of MPER (C-MPER) based on cryo-EM reconstructions of native Env complexes[17]. Back contours are derived from detergent-solubilized Env trimers, without (right, EMDB-3308) or with 10E8 bound (left, EMDB-3312). Transition between both states would result in accessibility to MPER helix in native Env (green). **(b)** Structural model for 10E8 recognition of the helical C-MPER epitope inserted in membranes. The position of the TMD residues (blue) was rendered by superimposing residues N671-V689 of MPER in complex with Fab 10E8 (PDB ID: 5GHW) onto structures of MPER-TMD peptides (PDB ID: 2MG1, 2MG2). Numbers denote the interaction-accommodation surfaces in the Fab after binding to C-MPER epitope (see main text). **(c)** Schematics of the liposome-peptide vaccines used in this study, which contain the reconstituted CpreTM-TMD peptide (in ribbon representation, lysine tag depicted in yellow). Left panel: numbers denote the attempt to recover through vaccination antibodies that bind to C-MPER epitope (1); and develop a surface to accommodate the membrane interface (2). Right panel: antigenic face of the C-MPER helix. Main epitope residues that interact with the 10E8 paratope are depicted in stick representation.

Functional characterization of bnAb 10E8 variants used to assess C-MPER exposure.

Fab 10E8 binding to membranes containing CpreTM-TMD reflects the accessibility to the C-MPER epitope at the membrane surface. As explained above, Fab binding implies not only the adequate fitting of the specificity pocket of the antibody to its MPER epitope, but also the correct positioning of the antibody at the membrane interface. Thus, in our approach we assumed that alteration of the Fab surface that accommodates the membrane interface might promote or diminish the capacity of 10E8 to bind its epitope. Following this rationale we generated two Fab 10E8 variants that, along with the WT Fab, were used as standard references to gauge the correct membrane topology of the C-MPER epitope (Figure 2a). The LC.S65W mutation added a Trp at the Fab surface that accommodates the viral membrane, and was expected to enhance the binding of the Fab to Env by increasing its affinity for the membrane interface [35, 41]. Conversely, the HC.W100bD mutation was designed to interfere with the membrane insertion of the heavy chain complementarity-determining region 3 loop (HCDR3) of the Fab [19, 42].

Super-resolution fluorescence microscopy experiments confirmed the differential binding of the 10E8-based Fabs to native Env on intact virions [35]. Quantitative stimulated emission depletion (STED) microscopy offers a spatial resolution of < 40 nm, below the size of HIV virions (around 125 nm), which allowed us to unequivocally identify the antibody signal coming from viral particles and resolve features within them [43]. Moreover, due to the linear nature of STED microscopy, the number of photons recorded is directly proportional to the amount of fluorescent molecules, which permitted quantification of antibody binding [35]. Figure 2b displays microscopy images of individual Vpr.EGFP-labeled viral particles incubated with Fab 10E8 WT or its

variants, LC.S65W and HC.W100bD (left panels), whose binding to Env on the particles was visualized by directly labeling Fabs with the STED-able Aberior STAR RED (also known as KK114) dye and also using a STAR RED-labeled secondary antibody.

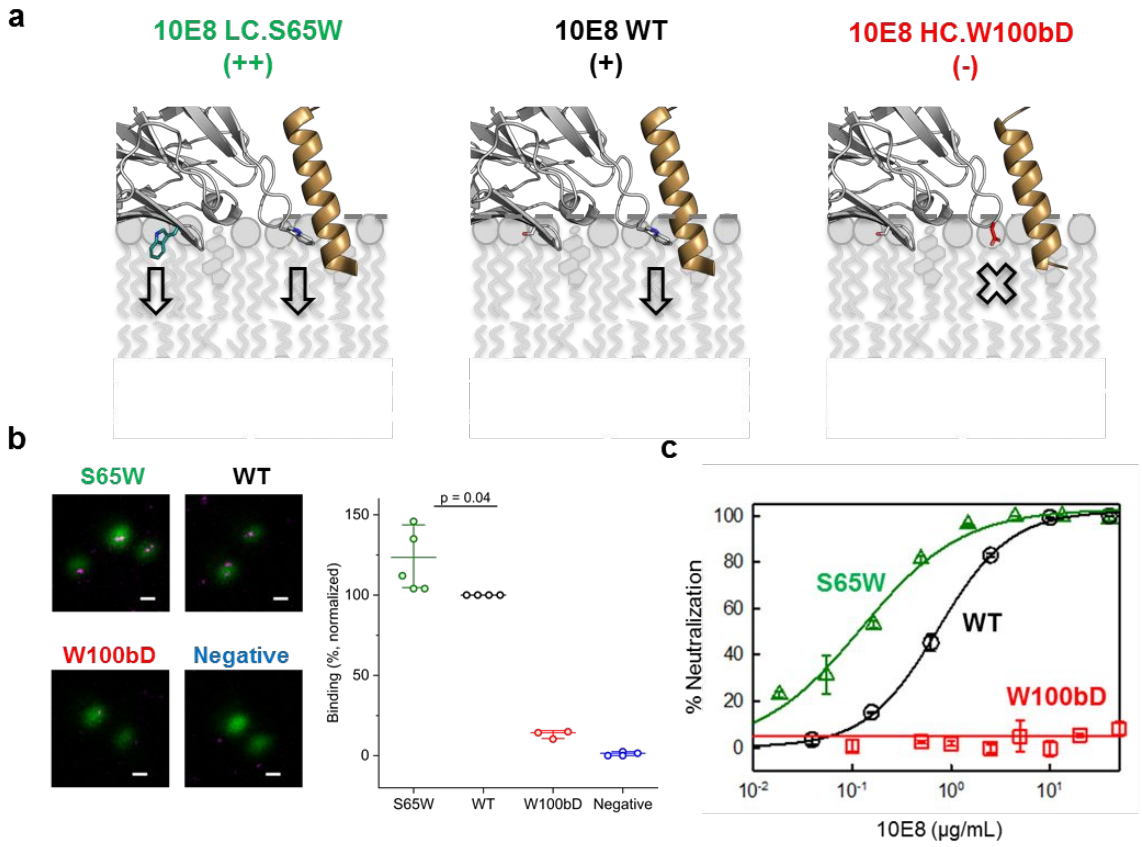

Figure 2: Functional properties of Fab 10E8 variants. (a) Structural model of gp41 C-MPER at the membrane interface in complex with Fab 10E8 WT (PDB ID: 5GHW, middle panel). LC.S65W and HC.W100bD variants are depicted in left and right panels, respectively. HC.W100b residue and mutated residues LC.S65W and HC.W100bD are displayed in stick representation. Arrows indicate the potential capacity of each Fab to anchor to the membrane. **(b)** Binding of Fab 10E8 WT and its mutants to native Env, measured by quantitative STED microscopy. Left: micrographs of HIV virions (EGFP.Vpr confocal signal, green) and 10E8 variants (STAR RED, magenta). Scale bar is 200 nm. Right: STED intensity signals (sum of collected photons) detected on single virions for each antibody were normalized to the signal of Fab WT after background subtraction. Each point is an independent experiment, middle horizontal bar represents the median and whiskers the SD. The number of individual virions analyzed in every experiment was at least 150 and typically around 400 for every condition (See Supplementary Figure S2 for single virus data). Negative corresponds to viruses untreated with Fabs. **(c)** Neutralization potency of 10E8 Fab variants. Dose-response curves follow cell entry inhibition measured against HIV-1 virions pseudotyped with JR-CSF Env. Data for WT, LC.S65W and HC.W100bD are shown with circles (black), triangles (green) and squares (red), respectively, and correspond to mean values (±SD) from two replicate wells in a representative experiment.

As hypothesized, quantitative analysis of the antibody signal in individual virions followed the trend: 10E8-LC.S65W > 10E8-WT > 10E8-HC.W100bD, with an average 24% increased binding of the LC.S65W variant to Env as compared to the WT version, and an 87% binding decrease of the HC.W100bD mutant (Figure 2b right panels and Figure S2). The capacity of these Fab 10E8 variants to bind to MPER on intact virions further correlated with their neutralization potency (Figure 2c). Therefore, we conclude that this binding pattern has to be reproduced by any relevant peptide epitope proposed as a vaccine candidate targeting 10E8-like antibody responses.

C-MPER accessibility in liposome vaccines containing reconstituted CpreTM-TMD:

Chol acts as modulator of the structure-function of integral membrane proteins, thereby affecting the exposure of cell surface/membrane anchored therapeutic targets such as GPCRs, ion channels, transporters, or growth factor receptors [44-45]. Folding of the gp41 MPER-TMD region also takes place in the Chol-enriched environment of the viral membrane[46-47], hence, this compound is assumed to play a role in C-MPER immunogenicity and its molecular recognition by 10E8. Furthermore, the stability and immunogenicity of liposome-based vaccine formulations are customarily enhanced by inclusion of Chol in the lipid composition [14]. Using the Fab 10E8 variants described in the previous section, we next determined the exposure of the C-MPER epitope in liposome-peptide formulations (LPFs) proposed as vaccines, which consisted of the CpreTM-TMD peptide reconstituted into liposomes composed of POPC:PA and 0, 20, 40 or 50 % Chol (Figure 3). LPFs were generated by mixing the CpreTM-TMD peptide with POPC:PA:Chol lipids in organic phase prior to generation of the liposome

particles. Sucrose density gradient ultracentrifugation proved full incorporation of CpreTM-TMD to membranes after the reconstitution procedure (Figures S3). Moreover, the resulting LPFs did not differ significantly in size (Figure S4).

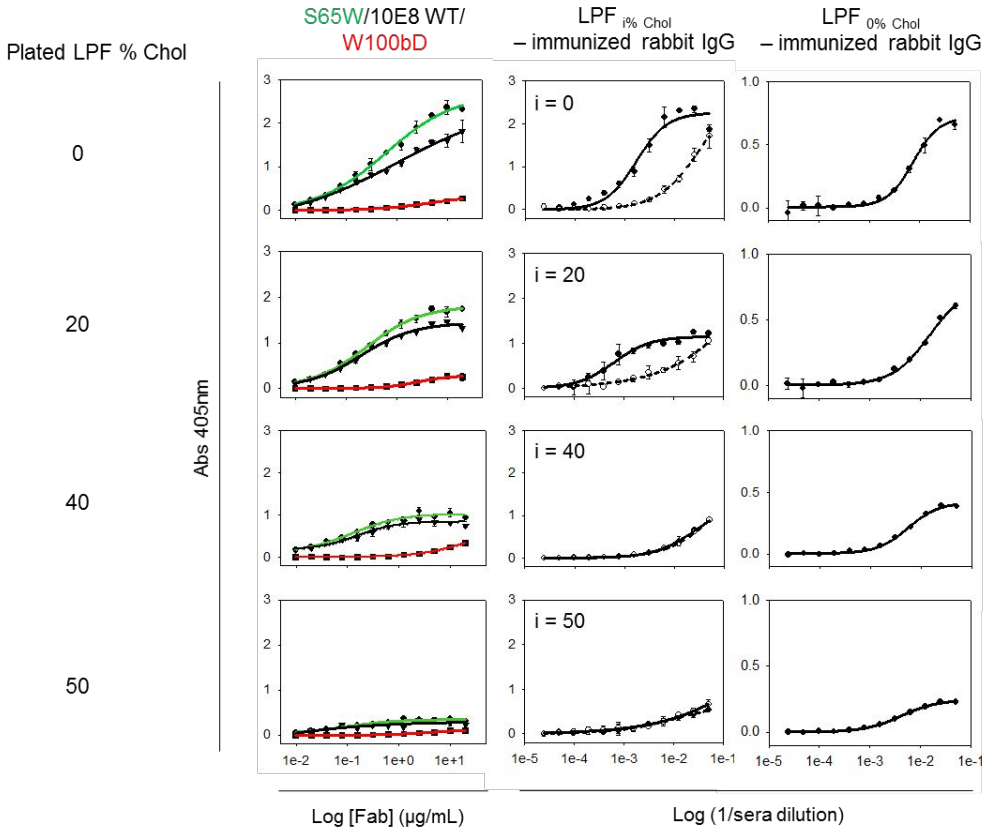

Figure 3. Antigenic profile and immunogenicity of liposome-peptide formulations. ELISAs were performed with liposome-peptide formulations (LPFs) containing CpreTM-TMD (peptide-to-lipid mole ratio, 1:50) that were coated on plates at a concentration of 500 µM and containing increasing concentrations of Chol as indicated in the panels. Plotted absorbance values are means (±SD) from two replicate wells. Left panels: comparative binding of Fab 10E8 variants WT (black line and filled triangles), LC.S65W (green line and filled circles) and HC.W100bD (red line and filled squares). Middle panels: immunogenicity of LPFs, as measured by the presence of IgG antibodies in the sera of two different rabbits after immunization. Signal of the pre-immune sera was subtracted. Right panels: cross-reactivity of IgG produced in sera of rabbits immunized with LPFs devoid of cholesterol, against LPFs with increasing cholesterol concentration. Sera from the two animals were pooled and the IgG levels in the mixture subsequently detected by ELISA. In all cases, experimental values were adjusted to sigmoid dose-response curves.

Binding of Fab 10E8 variants to LPFs coated on ELISA plates followed in all instances the expected trend for a correctly exposed epitope: 10E8-LC.S65W > 10E8-WT > 10E8-HC.W100bD, but the binding levels decreased greatly in samples containing the

highest Chol concentrations (Figure 3, left panels). Thus, high doses of Chol seemed to conceal the 10E8 epitope of the reconstituted CpreTM-TMD peptide. Similar results were obtained for KK114-labeled 10E8 variants interacting with CpreTM-TMD peptide reconstituted in Giant Unilamellar Vesicles (GUVs) made of the same lipid mixtures (Figure S5).

A similar trend was observed for the serum IgG produced after immunization of rabbits with the LPF vaccines. Thus, the amount of IgG that bound to LPF immunogens also decreased with the content of Chol present in the formulations (Figure 3, center panels). Interestingly, IgG produced in rabbits immunized with the LPF devoid of Chol, also trended to lower binding to the LPFs containing increasing concentrations of Chol (Figure 3, right panels). Thus, Chol may have restricted the accessibility of B-cell receptors to C-MPER, and also that of the IgGs produced upon immunization with LPFs bearing an accessible C-MPER epitope.

Stability of liposome vaccines with reconstituted CpreTM-TMD

Membrane-active peptides can generate fusion-related perturbations in lipid bilayers [5]. We have previously reported that pre-loading Chol-enriched vesicles with CpreTM rendered them competent for subsequent lipid-mixing with target vesicles [23, 25]. Therefore, CpreTM can alter the membrane integrity of Chol-enriched membranes to make them competent for fusion. Since vesicle fusion with cellular membranes might diminish the fraction of C-MPER epitope accessible for engagement with the components of the immune system, we next analyzed whether CpreTM-TMD-containing liposome vaccines were also inherently unstable and prone to fusion (Figure 4a).

To test this, we used a heterotypic fusion assay, in which GUVs that mimicked the composition and curvature of the cell plasma membrane external leaflet were the targets for LPFs primed for fusion by incubation with C-MPER containing peptides. Incubation of GUVs with CpreTM-primed LPFs led to the homogeneous labeling of the GUV membranes with the fluorescent LPF label, indicative of LPFs mixing their membrane lipids with those of GUVs. Consistent with previously published bulk measurements [23, 25], this effect was only observed when CpreTM was administered together with vesicles containing high concentrations of Chol. Conversely, incubation of fluorescently-labeled CpreTM-TMD liposome vaccines with target GUVs did not lead to dye transfer under any condition, demonstrating that CpreTM-TMD-containing LPFs are not prone to fusion, not even when they contain a high proportion of Chol.

To inquire whether the non-fusogenic CpreTM-TMD peptide reconstituted in Chol-containing membranes could still perturb locally the integrity of the lipid bilayer, we next determined the permeability of the membranes composing the different LPF vaccines also using a single-vesicle approach [48]. Confocal micrographs of GUVs matching the lipid composition of the LPFs, and containing CpreTM-TMD are depicted in Figure 4b. In addition, vesicles lacking peptide or vesicles treated with the peptide CpreTM were used as a control for negative permeabilization or effective permeabilization, respectively [22, 48]. Both untreated and CpreTM-TMD-containing GUVs were viewed as dark (empty) spheres surrounded by the NBD-labeled lipid bilayer (depicted in green color), against a background containing the permeant KK114 fluorescent probe, (rendered in red color). In contrast, incubation with the CpreTM peptide resulted in the red labeling of the internal compartments, consistent with the permeabilization of the lipid bilayer to the dye in the external solution [48].

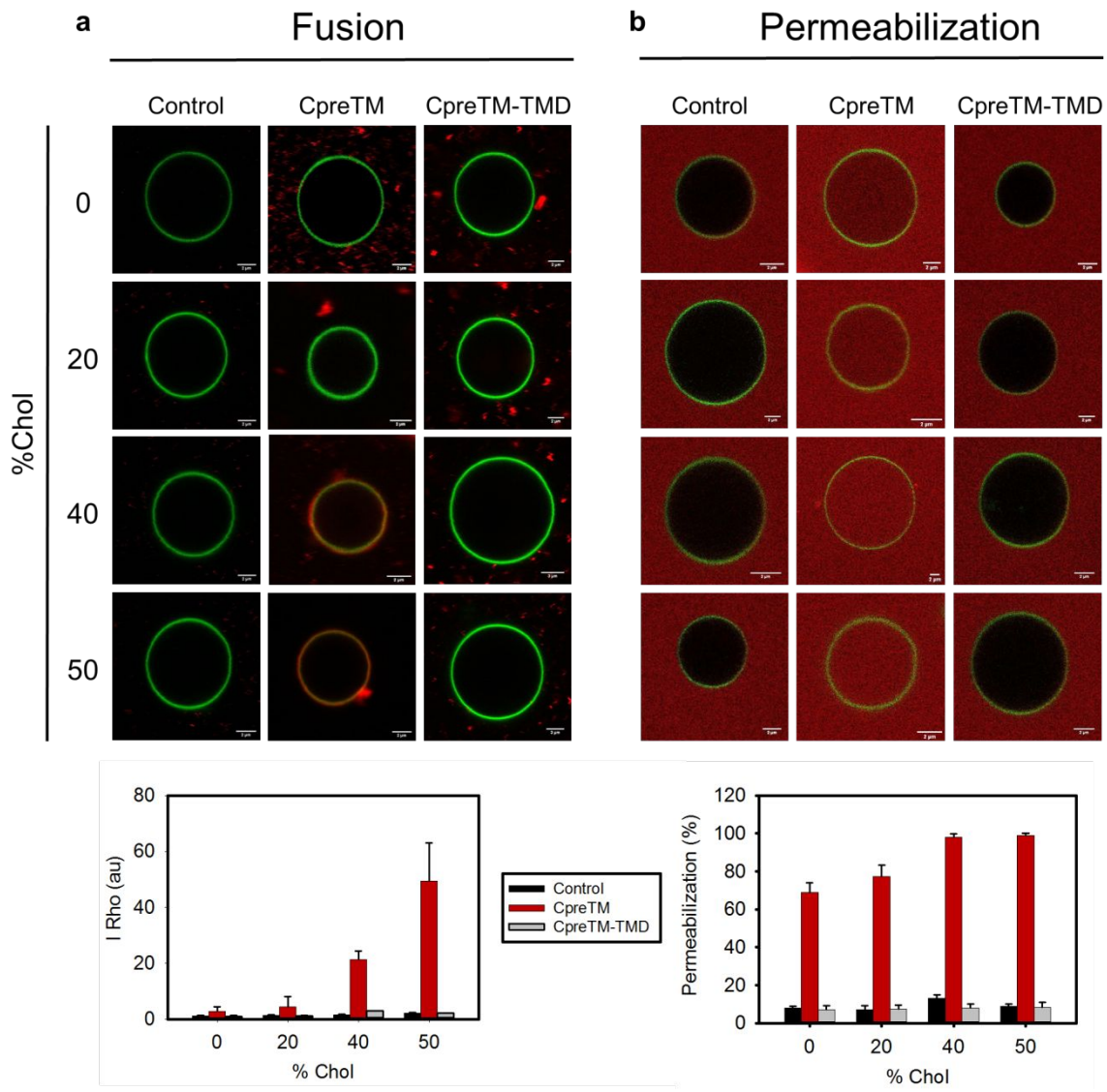

Figure 4: Stability of CpreTM-TMD-containing lipid bilayers measured in single-vesicle assays. (a) Channel-merged confocal fluorescence microscopy images of a heterotypic fusion assay between NBD-labeled GUVs mimicking the outer leaflet of cell plasma membrane (green) and Rho-labeled LPFs of varying cholesterol concentrations (red) in the absence (control) or presence of CpreTM or CpreTM-TMD peptides (1:50 peptide-to-lipid mole ratio). Rhodamine dye transfer to GUV membranes is indicative of lipid-mixing. The bottom plot shows the relative extents of fusion obtained by measuring the fluorescence intensity of the Rho dye at the membrane of each GUV after co-incubation with LUVs for 60 min (mean fluorescence values ± SD of 5 different vesicles per composition). **(b)** Channel-merged micrographs of single GUV permeabilization assays. NBD-labeled GUVs matching the lipid composition of the LPFs (green circumferences) and containing CpreTM, CpreTM-TMD or no peptide, were immersed in a solution containing the water soluble KK114 fluorescent probe (red background). The presence of KK114 inside the vesicles indicates effective permeabilization. The bottom plot shows relative permeabilization levels after 60 min incubation (mean fluorescence values ± SD of 5 different vesicles per composition).

Even though the absence of bilayer perturbations in samples that contained CpreTM-TMD was apparent after microscopic examination, we also performed quantitative measurements of fluorescence in selected GUVs (lower panels of Figure 4). These data further illustrate the absence of peptide-induced effects (i.e., ground-like levels of Rho or KK114 fluorescence in membrane or lumen, respectively).

Lipid packing changes and peptide conformational transitions in LPFs

Overall, the previous results demonstrate that the reconstituted CpreTM-TMD peptide is devoid of the membrane activity of the CpreTM section, suggesting that membrane restructuring is not the cause of the C-MPER epitope concealment observed in Chol-rich LPFs. Chol also induces a dose-dependent lipid packing increase when incorporated into lipid bilayers [49]. It has been suggested that the ‘‘cholesterol recognition/interaction amino acid consensus’’ motif ^{679}LWYIK/R^{683} present in CpreTM-TMD could sequester Chol[24, 50], and interfere with lipid packing, making bilayers more fluid, a biophysical effect that may condition immunogenicity of the LPFs[14]. Thus, we next performed two-photon fluorescence imaging of Laurdan-stained GUVs to quantitatively determine lipid packing in the liposome-based vaccines that contained different amounts of Chol [24, 47]. The emission spectrum of Laurdan changes in response to polarity. In a membrane context, changes in polarity are ascribed to differences in lipid packing, which influences water accessibility. The Generalized Polarization (GP) ratiometric parameter quantifies Laurdan’s emission spectral shift from tightly packed bilayers (high GP value) to loosely packed membranes (low GP value), thus providing an *in situ* estimation of membrane packing.

Figure 5a displays GP images of POPC:PA GUVs containing increasing Chol concentrations. The bottom panels include vesicles that incorporated the reconstituted CpreTM-TMD peptide. Mean average GP values increased with Chol concentration in the samples, as expected from the ordering effect exerted by this compound in lipid bilayers. Besides, the measured GP values demonstrated that incorporation of the peptide had little effect on membrane order levels, ruling out that the reconstitution process and/or potential specific interactions with Chol could affect lipid packing in LPFs.

It has been additionally argued that lipid packing augmented by Chol can affect the accommodation of the transmembrane helices[49, 51]. Thus, we next established the influence of Chol on the conformation adopted by CpreTM-TMD in LPF vaccines (Figure 5b). Infrared spectra in the amide-I region of CpreTM-TMD reconstituted in POPC:PA LPFs exhibited absorption centered at 1654 cm^{-1}, indicative of a main α-helical conformation adopted by the peptide[52]. Appearance of a shoulder could be discerned in LPF samples that contained increasing amounts of Chol, which was evidenced as a band centered at ca. 1620 cm^{-1} at the highest concentration of the compound. The growth of this band component reflected accumulation of extended chains, a product of peptide partial unfolding. Spectral changes could also be observed within the 1670-1660 cm^{-1} range, ascribed to absorption by conformers rich in 3_{10}-helix and turns. A relative contribution of the different conformations to the overall CpreTM-TMD structure in membranes was obtained after band decomposition of the LPF spectra (Figure S6).

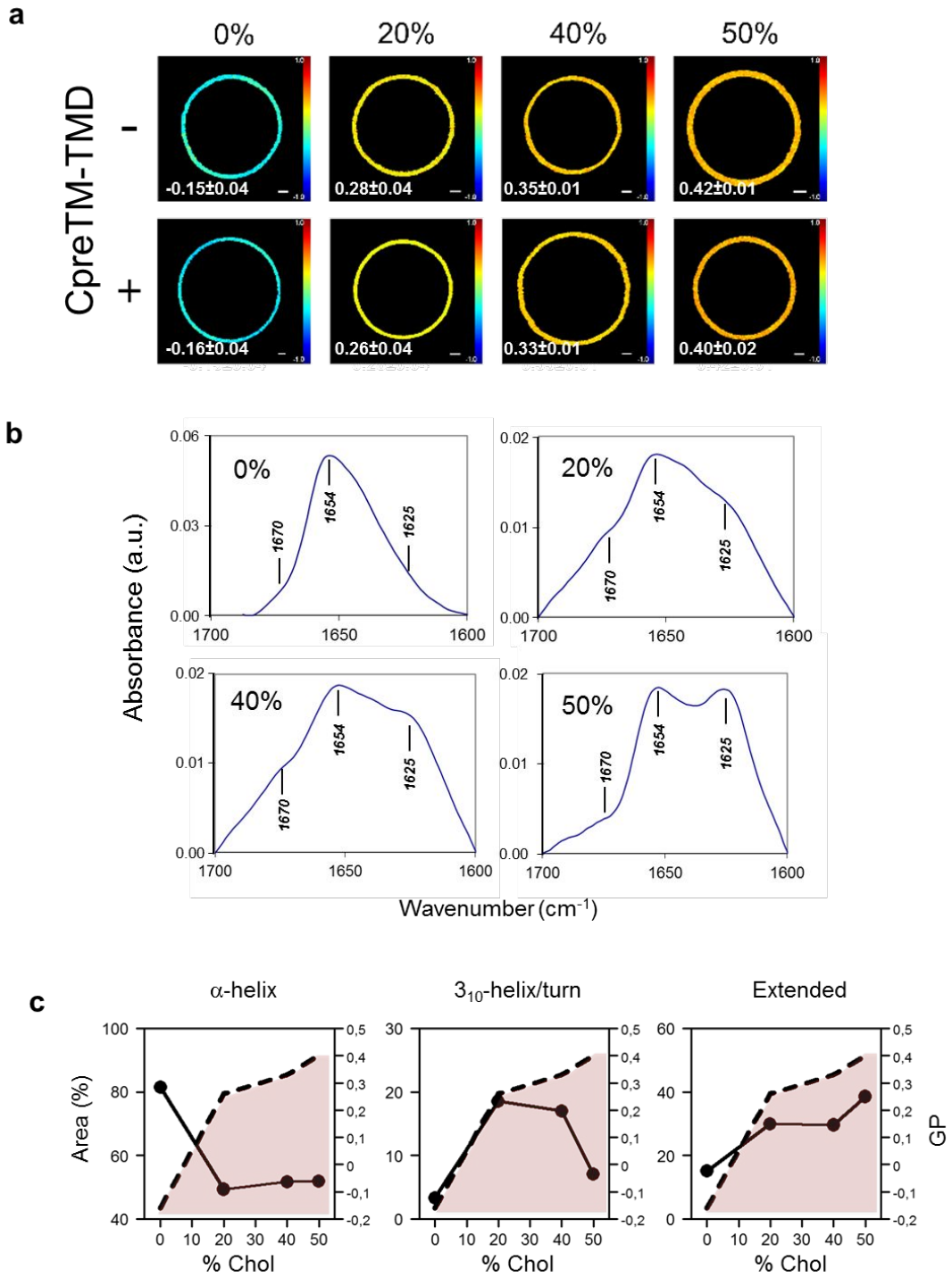

Figure 5: Lipid packing and structure of CpreTM-TMD in liposome-based formulations. **(a)** Laurdan GP images of single GUVs containing increasing cholesterol concentrations (0, 20, 40 or 50 mol %) with reconstituted CpreTM-TMD or in the absence of the peptide. High GP values (red) correspond to high molecular packing as opposed to lower GP values (blue) corresponding to more loosely packed membranes. Mean GP values ± SD of more than 30 GUVs of two independent experiments are shown in the panels. Scale bar is 1 µm. **(b)** IR spectra in the amide-I region of CpreTM-TMD reconstituted in LPFs containing increasing Chol concentrations. **(c)** Correlation between changes in CpreTM-TMD conformation (%Area), and lipid packing degree (Laurdan GP values). Contribution of the secondary structure components was calculated after IR amide-I band decomposition (Figure S6).

Figure 5c illustrates the evolution of the different structural components (percentage of amide-I band area) as a function of the Chol content and lipid packing (GP value). The data suggest that an initial sharp increase in lipid packing correlates with a reduction of the α-helix content and an increment in the contribution of 3_{10}-helix and turns, consistent with the partial destabilization of the main helical conformation in the samples. Further addition of Chol resulted in accumulation of extended structures and reduction of 3_{10}-helix and turns. Together, the IR results suggest that Chol can alter gradually the conformation of the CpreTM-TMD helix inducing its partial unfolding.

Model for Chol-induced C-MPER epitope disruption

It has been recently described that TMDs with smaller solvent accessible surface areas accommodate more efficiently in highly packed membranes than those rich in bulkier residues.[51] Consequently, most of the TMD helices found to reach the plasma membrane in eukaryote cells tend to segregate amino acids asymmetrically in two regions[53]: residues containing short and less bulky side chains locate in the section that passes through the highly packed exoplasmic leaflet, whereas those with the more voluminous side chains, tend to remain in contact with the internal monolayer, where the disorder of the acyl chains is higher. This trend is reflected by the Surface $Area_{exoplasmic}$/Surface $Area_{endoplasmic}$ parameter, which measures the ratio of exoplasmic to cytoplasmic lipid-accessible surface areas of the helix[53]. The value of this parameter is significantly less than 1 in the TMDs anchored to the plasma membrane.

Remarkably, as shown in Figure 6a, the Surface $Area_{exoplasmic}$/Surface $Area_{endoplasmic}$ parameter calculated for the helix spanning the CpreTM-TMD region of HIV-1 is ca. 1.6, i.e., significantly higher than 1. Therefore, the CpreTM-TMD section rich in bulky residues is more prone to unfold in tightly packed lipid bilayers than the rest of the TMD region due to its comparatively larger surface area. We surmise that the increase in lipid packing causes the conformational changes of the MPER-TMD helix that result in the disruption of the C-MPER epitope (Figure 6b).

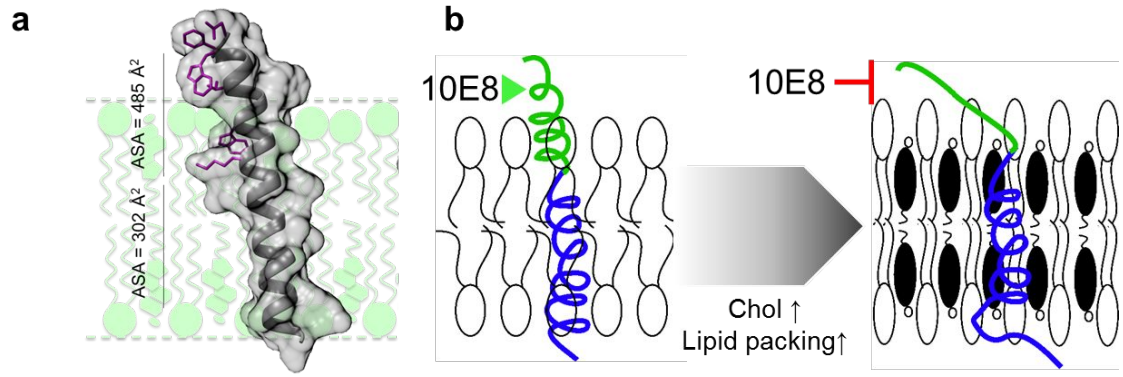

Figure 6: Model for restricted accessibility to C-MPER epitope in Chol-enriched membranes. (a) Asymmetry of CpreTM-TMD transmembrane helix surface area between halves of the lipid bilayer. Accessible surface areas were calculated as described[51, 54]. **(b)** Cartoon illustrating unfolding of the CpreTM-TMD helix section containing the C-MPER epitope upon lipid-packing increase. Note that the model does not exclude chain extension also occurring at the C-terminal side of the helix, as previously proposed[13].

DISCUSSION

The relevance of the C-MPER epitope as a target for vaccine design is highlighted by the discovery that broad and potent HIV-1 neutralizing activity of sera collected from chronically infected individuals can be in part mapped to this subregion [26, 55-61]. Despite the interest in developing effective immunogenic formulations, as a general rule, vaccines against this site, are poorly immunogenic[14]. The available structural information on the mechanism of HIV bnAb binding to native C-MPER, suggests that

an effective vaccine should elicit antibodies that i) engage with the integral membrane antigen Env, ii) develop the ability to recognize specifically residues exposed on the accessible face of the C-MPER helix, and iii) develop a surface to accommodate the viral membrane interface (Figure 1).

To formulate properly the C-MPER sequence at membrane surfaces, in this work we have followed a new strategy (Figure S1). First, to focus immune responses to a single epitope, the selected CpreTM-TMD peptide contains only the C-terminal subdomain of MPER, which is followed by a minimal Env TMD that can effectively anchor the protein in the membrane[40]. We note that peptides containing the full MPER sequence appear to occlude the C-MPER sequence in the membrane interface[13, 62], and tend to raise responses focused on the N-terminal subdomain when formulated as LPFs (i.e., produce antibodies against the 2F5 epitope, but not against the 10E8 epitope)[62].

Second, we have generated functional variants of 10E8 and used them to gauge the correct presentation of 10E8 epitope in LPFs. Our data indicate that LPFs containing CpreTM-TMD are recognized by 10E8 variants following their functional profile. Furthermore, these formulations are immunogenic in rabbits, demonstrating their capacity to engage with B-cell receptors.

Third, we have altered the lipid composition of the membrane and evaluated its effect on the antigenicity and immunogenicity of LPFs. It has been argued that a virus-like membrane environment should be preserved in the conception of peptide vaccines targeting the C-terminal region of MPER [14, 36]. Thus, we used increasing concentrations of Chol in the lipid mixtures in order to mimic the tight lipid packing of the viral membrane[47]. The antibody-based experiments revealed that C-MPER gets occluded in the Chol-rich membranes, in line with the trend revealed by the immunogenicity assays.

Consistent with this notion, recently published data indicate that the 10E8 epitope is more accessible in cyclodextrin-treated virions, which purportedly contain lower amounts of Chol[63].

Given the crucial importance of the lipid composition in the development of a LPF MPER vaccine, we further investigated the molecular basis for the Chol-induced 10E8 epitope occlusion. Our data demonstrate that the lipid bilayers containing the reconstituted CpreTM-TMD peptide are stable in all compositions. However, the increase in lipid packing induced by Chol appears to directly affect C-MPER helix accommodation, provoking its unfolding and the loss of antigenicity.

Under the assumption that to ensure reproducibility and lower cost, simple lipid compositions would be preferred over complex lipid mixtures to manufacture liposome-based vaccines[14, 64], in this work we have used a single lipid, Chol, to adjust lipid packing. Nevertheless, other components of the HIV membrane such as sphingomyelin (SPM) and aminophospholipids (phosphatidylserine/phosphatidylethanolamine)[46], can increase membrane packing as determined by the Laurdan GP value[47]. Thus, although their ordering effects are less pronounced than those of Chol, in principle these lipids could also interfere with MPER exposure at membrane surfaces. However, it is well established that under certain conditions complex lipid mixtures that combine Chol with low melting T^a phospholipids, and high melting T^a SPM, can undergo lateral segregation generating Chol-rich (rigid) and Chol-depleted (fluid) domains in membranes (see for instance [65]). Therefore, despite the high Chol content of the HIV membrane and the presence of other lipids that enhance packing, it cannot be excluded an effective recognition of the MPER epitope by antibodies and BCRs occurring within the segregated fluid domains.

Finally, we can speculate on whether the structures observed, and the effect of Chol, provide some insight into the structure-function of Env. In this respect, a crystal structure of the 6-helix bundle containing the full MPER sequence supports the adoption of an extended conformation by MPER residues within an Env fusion intermediate[66]. Thus, we surmise that a tendency for alternating the helical conformation of the MPER-TMD region with more flexible and extended structures, might help completing the structural changes undergone by the gp41 ectodomains upon fusion activation of the Env trimer (last step in Figure S1a).

CONCLUSION

Our goal in this work was to provide new pathways for the design of antiMPER vaccines. Together, our results suggest that the reconstitution process stabilizes a transmembrane CpreTM-TMD α-helix, exposing to solvent an accessible C-MPER epitope. The increase of lipid packing induced by Chol appears to promote more readily unfolding of the solvent-exposed and bulkiest section of the CpreTM-TMD helix causing disruption of the C-MPER epitope. Thus, we infer that the increase in Chol may force extrusion-extension of the C-MPER section to accommodate the peptide chain, and induce the concomitant disorganization of the 10E8 epitope at the membrane interface (Figure 6). In conclusion, our observations underpin the use of CpreTM-TMD-based sequences in future designs of MPER-targeting vaccines [14], but, contrary to common perception, they caution that reconstituted peptides aimed to focus immune responses to the pan-neutralizing HIV-1 C-MPER sub-region should be formulated in membranes devoid of Chol.

METHODS

Reagents:

The peptide sequences derived from the gp41 MPER-TMD region, *KKK*-NWFDITNWLWYIKLFIMIVGGLV-*KK* (CpreTM) and *KKK*-NWFDITNWLWYIKLFIMIVGGLVGLRIVFA-*KKKK* (CpreTM-TMD) were produced by solid-phase synthesis using Fmoc chemistry as C-terminal carboxamides and purified by HPLC. 1-palmitoyl-2-oleoyl-*sn*-glycero-3-phophocholine (POPC), phosphatidic acid (egg, chicken) (PA), cholesterol (Chol), sphingomyelin (egg, chicken) (SM) and Lipid A detoxified (*Salmonella minnesota* R595) were purchased from Avanti Polar Lipids (Birmingham, AL, USA). N-(7-nitro-benz-2-oxa-1,3-diazol-4-yl)phosphatidylethanolamine (N-NBD-PE), N-(lissamine Rhodamine B sulfonyl)phosphatidylethanolamine (N-Rh-PE) and 6-dodecanoyl-2-dimethylaminonaphthalene (Laurdan) fluorescent probes were from Thermo Fisher Scientific (Waltham, Massachusetts, USA). Abberior STAR RED (KK114) was obtained from Abberior (Göttingen, Germany). Goat anti-Human IgG (Fab specific) – AP was obtained from Invitrogen (Carlsbad, California, USA) and goat anti-Rabbit IgG – AP from Thermo Fisher Scientific (Waltham, Massachusetts, USA).

Production of Fab 10E8 and its variants

Fab 10E8 antibody sequences was cloned in the plasmid pColaDuet and expressed in *Escherichia coli* T7-shuffle strain. Recombinant expression was induced at 18 °C overnight with 0.4 mM isopropyl-D-thiogalactopyranoside when the culture reached an optical density of 0.8. Cells were harvested and centrifuged at 8,000 × *g*, after which they were resuspended in a buffer containing 50 mM HEPES (pH 7.5), 500 mM NaCl,

35 mM imidazole, DNase (Sigma-Aldrich, St. Louis, MO) and an EDTA-free protease inhibitor mixture (Roche, Madrid, Spain). Cell lysis was performed using an Avestin Emulsiflex C5 homogenizer. Cell debris was removed by centrifugation, and the supernatant loaded onto a nickel-nitrilotriacetic acid (Ni-NTA) affinity column (GE Healthcare, Chicago, Illinois, USA). Elution was performed with 500 mM imidazole, and the fractions containing the His-tagged proteins were pooled, concentrated and dialyzed against 50 mM sodium phosphate (pH 8.0), 300 mM NaCl, 1 mM DTT, and 0.3 mM EDTA in the presence of purified protease Tobacco etch virus [67]. Fabs were separated from the cleaved peptides containing the His_{6x} tag by an additional step in a Ni-nitrilotriacetic column. The flow-through fraction containing the antibody was dialyzed overnight at 4 ºC against sodium acetate (pH 5.6) supplemented with 10% glycerol and subsequently loaded onto a MonoS ion exchange chromatography (IEC) column (GE Healthcare, Chicago, Illinois, USA). Elution was carried out with a gradient of potassium chloride and the fractions containing the purified Fab concentrated and dialyzed against a buffer containing 10 mM sodium phosphate (pH 7.5), 150 mM NaCl, and 10% glycerol. For the preparation of mutant Fabs, the KOD-Plus mutagenesis kit (Toyobo, Osaka, Japan) was employed following the instructions of the manufacturer. For confocal microscopy experiments, position $C216_{HC}$ of the fabs was modified *in vitro* with a sulfhydryl-specific iodacetamide derivative of the KK114 probe.

Functional characterization of Fab 10E8 and its variants

Pseudovirus production

HIV-1 pseudoviruses were produced by transfection of human kidney HEK293T cells with the full-length env clone JR-CSF (kindly provided by Jamie K. Scott and Naveed Gulzar, Simon Fraser University, BC, Canada) using calcium phosphate. Cells were co-transfected with vectors pWPXL-GFP and pCMV8.91, encoding a green fluorescent protein and an env-deficient HIV-1 genome, respectively (provided by Patricia Villace, CSIC, Madrid, Spain). For imaging experiments, pWPXL-GFP was replaced by pEGFP.Vpr (NIH AIDS Reagent Program). After 24 h, the medium was replaced with Optimem-Glutamax II (Invitrogen Ltd, Paisley, UK) without serum. Two days after transfection, the pseudovirus particles were harvested, passed through 0.45 μm pore sterile filters (Millex® HV, Millipore NV, Brussels, Belgium) and finally concentrated by ultracentrifugation in a sucrose gradient at 24.000 rpm for 2h.

Super-resolution STED microscopy

EGFP.Vpr-labeled virions were immobilized on 0.1% poly-L-lysine coated coverslips after 10 min incubation. Coverslips were then blocked with 2% BSA and antibodies incubated in blocking buffer for 1 h at a concentration of 25 μg/ml (ca. 0.5 μM). In the case of unlabeled Fabs, the samples were incubated for an extra hour with donkey anti-human STAR RED antibodies (1/200 dilution). Finally, samples were fixed with 2% PFA and mounted in Mowiol//DABCO mounting medium.

Imaging was performed using an Abberior STEDYCON system. STAR RED was excited using a 640 nm pulsed laser line and depleted with using a 775 STED laser. EGFP was excited with a 488 nm pulsed laser line. Emission was collected using avalanche photodiodes. The emission filters were 650-700 nm for the super-resolved STAR RED signal and 501-552 nm for the confocal EGFP signal. Pixel size was fixed at 20 nm pixel, dwell time was 10 μs and line accumulation was set to 5.

Only samples prepared in parallel and imaged within the same session were compared. To allow for comparison of independent experiments, intensity was normalized to the median 10E8 intensity after background noise subtraction. Image analysis was performed using the Python code developed previously[35, 68] and available at this site (DOI: 10.5281/zenodo.1465920). The software automatically identified EGFP.Vpr positive particles using an intensity-maximum finding algorithm on a Gaussian smoothed image (σ= 2.0), and quantified the number of collected photons in a circular region of interest of 14 pixels (280 nm) in diameter. It performed the same quantification in a random region presenting no Vpr.EGFP signal, which was used as a reference background signal.

Cell entry assays

HIV entry was determined using TZM-bl target cells (AIDS Research and Reference Reagent Program, Division of AIDS, NIAID, NIH, contributed by J. Kappes). Serial dilutions of Fabs were incubated for 1.5 h at 37 °C with a 10–15% tissue culture infectious dose of pseudovirus. Samples were set up in duplicate in 96-well plates. After antibody-pseudovirus co-incubation, 1,1 x 10^4 target cells were added in the presence of 30 µg/ml DEAE-dextran (Sigma-Aldrich, St-Louis, MO). Neutralization levels after 72 h were inferred from the reduction in the number of GFP positive cells as determined by flow cytometry using a BD FACSCalibur Flow Cytometer (BD Biosciences, San Jose, California, USA).

Liposome-peptide formulations

To prepare CpreTM-TMD containing LPFs, lipids and the CpreTM-TMD peptide were mixed in organic solvent prior to the production of the liposomes. Briefly, POPC, Chol

(0, 20, 40 or 50 mol %) and PA (5 mol %) were dissolved in chloroform:methanol 1:2 (vol:vol) and were mixed with CpreTM-TMD (dissolved in 100 % ethanol) at peptide-to-lipid molar ratio of 1:50. The mixture was dried under a N_2 stream and traces of organic solvents were removed by 2 h vacuum pumping. Subsequently, the dried lipid films were subjected to 2 h of gentle hydration with H_2O using a N_2 gas bubbler to facilitate the subsequent dispersion of the dried lipid-peptide film in PBS aqueous buffer. Next, the multilamellar vesicles were bath sonicated (1 h, 55 ºC) and subjected to 15 freeze and thaw cycles to obtain unilamellar vesicles. Chol concentration of liposome suspensions was determined by the cholesterol oxidase/peroxidase method (BioSystems, Barcelona, Spain), and found to be within the experimental error.

Rabbit immunization and response analysis by ELISA

New Zealand White rabbits were immunized at the antibody production service from the CID-CSIC (Barcelona, Spain). Liposome-based formulations were prepared following the methods described above including 0.25 mol % Lipid A as adjuvant [64] and were lyophilized. Two rabbits were inoculated intradermally at multiple sites on day 0 with 1 ml of each LPF sample reconstituted in pure water, which contained 0.4 mg peptide. Subsequent boosting injections, consisted of 1 ml of the reconstituted liposome formulation containing 0.3 mg peptide on day 21, while 0.2 mg of liposomal peptide were injected on day 42.

Enzyme-linked immunosorbent assay (ELISA)

LPFs were dissolved in phosphate-buffered saline (PBS) at a concentration of 500 μM and 1:50 CpreTM-TMD:lipid (mol:mol ratio) and immobilized (100 μl/well) overnight onto C96 Maxisorp microplate wells (Nunc, Denmark). The plates were blocked for 2 h

with 3 % (w/v) BSA in PBS and incubated with either the Fabs or rabbit sera for 4 hours. The binding of the Fabs or sera IgGs was detected by incubation for 50 min with 1:1000 dilution of alkaline phosphatase-conjugated goat anti-human IgG F(ab)2 (Invitrogen, Carlsbad, CA, USA) or goat anti-Rabbit IgG (Thermo Fisher Scientific (Waltham, MA, USA) respectively, which then catalyzed a color reaction for 30 min with 1 mg/mL p-nitrophenyl phosphate substrate (VWR International, Radnor, Pensilvania, USA) in 0.1 M glycine, 1 mM $MgCl_2$, 1mM $ZnCl_2$, pH 10.4, that could be measured by absorbance at a wavelength of 405 nm in a Synergy HT microplate reader (Bio-TEK Instruments Inc., VT, USA). The plates were extensively washed with PBS after each step.

Single-vesicle assays for membrane stability

Giant unilamellar vesicles were produced by spontaneous swelling as described by Velasco-Olmo et al. [69] In brief, 0.125 mg lipid was co-dissolved in 100 µL $CHCl_3$:CH_3OH (9:1) with the fluorescent probes Laurdan (1 mol %) or NBD-PE (2 mol %). When required, CpreTM-TMD peptide (dissolved in 100 % ethanol) was included in organic phase at 1:50 peptide-to-lipid ratio. The probe-containing lipid or lipid-peptide mixture was introduced in a vacuum desiccator for 1 h to remove the organic solvent and the desiccated lipid was hydrated with Milli-Q water for 1 h at temperatures above the transition temperature of the mixture (typically 55º C). 5 µL silica beads (40 µm) were then mixed with 20 µL of the MLV suspension, separated in 3.5 µL drops on a teflon film and vacuum dried for 1h. Dried beads covered with lipid were collected and transferred to an 85 g/L sucrose buffer in order to induce spontaneous swelling of GUVs. Finally vesicles were transferred to the observation dish in an isosmotic 10 mM Hepes, 150 mM KCl (pH 7.4) buffer.

For binding experiments, NBD-labeled GUVs with increasing concentrations of cholesterol and with or without the CpreTM-TMD peptide (1:50 peptide-to-lipid molar ratio) were used. The GUVs were added to a bovine serum albumin (BSA)-blocked microscope chamber that already included 250 nM of 10E8-based Fabs conjugated with the KK114 probe at residue $C216_{HC}$, and were incubated for 15 min prior to imaging.

For GUV-LUV heterotypic fusion experiments, NBD-labeled POPC:Chol:SM (2:2:1 mol:mol) GUVs devoid of peptide were added to a suspension of Rho-labeled LUV previously incubated with the CpreTM peptide or to a suspension of Rho-LPFs bearing CpreTM-TMD, both at 1:50 peptide-to-lipid molar ratio, and were incubated for 15 min prior to imaging.

For GUV permeabilization assays, NBD-labeled CpreTM-TMD-bearing GUVs were added to a BSA-blocked microscope chamber that already included the unconjugated and soluble KK114 dye, and were incubated for 15 min prior to imaging.

Confocal microscopy

Images were acquired on an inverted confocal fluorescence microscope (Nikon Eclipse TE-2000, Nikon, Nikon Instruments, Tokyo, Japan). NBD-stained GUVs, Rho-labeled LUVs and Fabs conjugated with the KK114 probe were excited at 476 nm, 514 nm and 637 nm, respectively. For GUV-LUV heterotypic fusion experiments, the fluorescence signal was collected into two different channels with band pass filters of 515/30 nm, and 590/94 nm. For binding and permeabilization experiments the band pass filters used were 515/30 and Long Pass 650 nm. The objective used was a 63X oleo immersion with a numerical aperture (NA) of 1.2.

Relative extents of Fab-GUV binding or LUV-GUV fusion were obtained by measuring the fluorescence intensity of KK114 or Rhodamine, respectively, along the equatorial

plane of the GUV images. Extents of permeabilization were calculated for each vesicle after 15 min incubation with KK114 following equation 1,

$$\text{Permeabilization (\%)} = \frac{F_{inside}}{F_{outside}} \times 100 \qquad \textit{Eq. 1}$$

where F_{inside} and $F_{outside}$ are the average of KK114 fluorescence intensities inside and outside a GUV, respectively. Fluorescence emission analyses were carried out with ImageJ software (rsb.info.nih.gov/ij/).

Membrane packing analysis by Multiphoton Fluorescence Microscopy

Images were acquired on a Leica TCS SP5 II microscope (Leica Microsystems GmbH, Wetzlar, Germany). For multiphoton excitation, the sample was illuminated with a 780 nm beam from a femtosecond-pulsed titanium-sapphire Mai-Tai Deepsee (Spectra-Physics, Berlin, Germany) laser. GUVs were imaged through a ×63 water-immersion objective (NA=1.2) and 512x512 pixel images were acquired at 400 Hz per scanning line. Fluorescence emission was collected by non-descanned (NDD) hybrid detectors, as they offer higher sensitivity compared to photomultipliers. NDD 1 collected the blue edge of the emission spectrum at 435 ± 20 nm and NDD 2 collected the red edge at 500 ± 10 nm. For Generalized Polarization (GP) measurements unilamellar GUVs were selected and imaged at the equatorial plane to avoid photoselection.

GP values were calculated using in-house developed software based on MATLAB (MathWorks, MA, USA) as described in our previous papers[24, 65]. After smoothing the images with a 2-pixel averaging circular filter and thresholding the intensity, GP values were calculated for every pixel on the image following equation 2,

$$GP = \frac{I_B - G \times I_R}{I_B + G \times I_R} \qquad Eq.\,2$$

where I_B is the intensity collected by NDD 1, I_R the intensity collected by NDD 2 and G is the factor that accounts for the relative sensitivity of the two channels, calibrated with 5 µM Laurdan solution in pure DMSO[65]. The mean GP value for each lipid mixture was calculated after imaging and analyzing at least 15 GUVs in each independent experiment.

Infrared spectroscopy

Infrared spectra were recorded in a Bruker Tensor 27 spectrometer equipped with a mercury-cadmium-telluride detector using a Peltier-based temperature controller (TempCon, BioTools Inc., Wauconda, IL) with calcium fluoride cells (BioCell, BioTools Inc., Wauconda, IL). LPFs were lyophilized and subsequently prepared at 3 mg/mL in D_2O buffer (PBS). A 25 µL sample aliquot was deposited on a cell that was sealed with a second cell. Reference windows without peptide were prepared similarly. Typically 1000 scans were collected for each background and sample, and the spectra were obtained with a nominal resolution of 2 cm^{-1}. Data treatment and band decomposition of the original amide I have been described elsewhere [52].

ANCILLARY INFORMATION

Supporting Information Available

Supporting Methods: description of the liposome-flotation assay. Supporting Figures S1-S6: This material includes a diagram to explain the strategy followed to focus immune responses to C-MPER epitope (Fig. S1), single virion-antibody binding data obtained from STED measurements (Fig. S2), determination of peptide incorporation to liposome vaccines through flotation experiments (Fig. S3), size polydispersity distributions of LPFs (Fig. S4), GUV-antibody binding data (Fig. S5) and secondary structure composition of CpreTM-TMD as a function of the Chol content in membranes (Fig. S6). Supporting bibliography

Corresponding author information

Correspondence and requests for materials should be addressed to BA (email: beatriz.apellaniz@ehu.eus) and to JLN (email: joseluis.nieva@ehu.es)

Author Contributions

B.A. and J.L.N. designed research; J.T, I.DA, P.C., S.I., E.R., E.L., and B.A., performed research; J.T., I.DA, P.C., E.R., E.L., C.E., J.L.R.A., B.A. and J.L.N. analyzed data; and B.A. and J.L.N. wrote the paper with input from all authors.

Acknowledgments

This study was supported by the following Grants: European Commission (790012 SI H2020-MSCA-IF-2017) (E.R., J.L.N.); Spanish MCI (RTI2018-095624-B-C21; MCI/AEI/FEDER, UE) (B.A., J.L.N.), Basque Government (IT1196-19) (B.A., J.L.N.). J.T. received a pre-doctoral fellowship from the Basque Government. PC acknowledges

a research associate contract at the University of the Basque Country (DOCREC18/01) and a postdoctoral fellowship from the Basque Government (POS_2018_1_0066). CE and PC acknowledge funding from the Deutsche Forschungsgemeinschaft (Research unit 1905, Jena Excellence Cluster "Balance of the Microverse", project no. 3162113987 – SFB 1278 (project C05)) and the Medical Research Council (MC_UU_12010/unit programmes G0902418 and MC_UU_12025). Technical assistance by Miguel García-Porras is greatly acknowledged.

Abbreviations Used: bnAb, broadly neutralizing antibody; GP, General Polarization; GUV, Giant Unilamellar Vesicle; LPF, Liposome-peptide formulation; LUV, Large Unilamellar Vesicle; MPER, Membrane-Proximal External Region; C-MPER, Carboxy-terminal subregion of MPER; TMD, Transmembrane Domain.

REFERENCES:

(1) Wyatt, R.; Sodroski, J., The HIV-1 envelope glycoproteins: fusogens, antigens, and immunogens. *Science* **1998,** *280* (5371), 1884-1888.

(2) Melikyan, G. B., Membrane fusion mediated by human immunodeficiency virus envelope glycoprotein. *Curr. Top. Membr.* **2011,** *68*, 81-106.

(3) Blumenthal, R.; Durell, S.; Viard, M., HIV entry and envelope glycoprotein-mediated fusion. *J. Biol. Chem.* **2012,** *287* (49), 40841-40849.

(4) Sanders, R. W.; Moore, J. P., HIV: A stamp on the envelope. *Nature* **2014,** *514* (7523), 437-438.

(5) Apellaniz, B.; Huarte, N.; Largo, E.; Nieva, J. L., The three lives of viral fusion peptides. *Chem. Phys. Lipids* **2014,** *181*, 40-55.

(6) Weissenhorn, W.; Dessen, A.; Harrison, S. C.; Skehel, J. J.; Wiley, D. C., Atomic structure of the ectodomain from HIV-1 gp41. *Nature* **1997,** *387* (6631), 426-430.

(7) Ozorowski, G.; Pallesen, J.; de Val, N.; Lyumkis, D.; Cottrell, C. A.; Torres, J. L.; Copps, J.; Stanfield, R. L.; Cupo, A.; Pugach, P.; Moore, J. P.; Wilson, I. A.; Ward, A. B., Open and closed structures reveal allostery and pliability in the HIV-1 envelope spike. *Nature* **2017,** *547* (7663), 360-363.

(8) Wang, H.; Barnes, C. O.; Yang, Z.; Nussenzweig, M. C.; Bjorkman, P. J., Partially Open HIV-1 Envelope Structures Exhibit Conformational Changes Relevant for Coreceptor Binding and Fusion. *Cell Host Microbe* **2018,** *24* (4), 579-592 e574.

(9) van Gils, M. J.; Sanders, R. W., Hitting HIV's Harpoon. *Immunity* **2018,** *49* (1), 14-15.

(10) Xu, K.; Acharya, P.; Kong, R.; Cheng, C.; Chuang, G. Y.; Liu, K.; Louder, M. K.; O'Dell, S.; Rawi, R.; Sastry, M.; Shen, C. H.; Zhang, B.; Zhou, T.; Asokan, M.; Bailer, R. T.; Chambers, M.; Chen, X.; Choi, C. W.; Dandey, V. P.; Doria-Rose, N. A.; Druz, A.; Eng, E. T.; Farney, S. K.; Foulds, K. E.; Geng, H.; Georgiev, I. S.; Gorman, J.; Hill, K. R.; Jafari, A. J.; Kwon, Y. D.; Lai, Y. T.; Lemmin, T.; McKee, K.; Ohr, T. Y.; Ou, L.; Peng, D.; Rowshan, A. P.; Sheng, Z.; Todd, J. P.; Tsybovsky, Y.; Viox, E. G.; Wang, Y.; Wei, H.; Yang, Y.; Zhou, A. F.; Chen, R.; Yang, L.; Scorpio, D. G.; McDermott, A. B.; Shapiro, L.; Carragher, B.; Potter, C. S.; Mascola, J. R.; Kwong, P. D., Epitope-based vaccine design yields fusion peptide-directed antibodies that neutralize diverse strains of HIV-1. *Nat. Med.* **2018,** *24* (6), 857-867.

(11) Salzwedel, K.; West, J. T.; Hunter, E., A conserved tryptophan-rich motif in the membrane-proximal region of the human immunodeficiency virus type 1 gp41 ectodomain is important for Env-mediated fusion and virus infectivity. *J. Virol.* **1999,** *73* (3), 2469-2480.

(12) Suarez, T.; Gallaher, W. R.; Agirre, A.; Goni, F. M.; Nieva, J. L., Membrane interface-interacting sequences within the ectodomain of the human immunodeficiency

virus type 1 envelope glycoprotein: putative role during viral fusion. *J. Virol.* **2000,** *74* (17), 8038-8047.

(13) Kwon, B.; Lee, M.; Waring, A. J.; Hong, M., Oligomeric Structure and Three-Dimensional Fold of the HIV gp41 Membrane-Proximal External Region and Transmembrane Domain in Phospholipid Bilayers. *J. Am. Chem. Soc.* **2018,** *140* (26), 8246-8259.

(14) Apellaniz, B.; Nieva, J. L., The Use of Liposomes to Shape Epitope Structure and Modulate Immunogenic Responses of Peptide Vaccines Against HIV MPER. *Adv Protein Chem. Struct. Biol.* **2015,** *99*, 15-54.

(15) Montero, M.; Gulzar, N.; Klaric, K. A.; Donald, J. E.; Lepik, C.; Wu, S.; Tsai, S.; Julien, J. P.; Hessell, A. J.; Wang, S.; Lu, S.; Burton, D. R.; Pai, E. F.; Degrado, W. F.; Scott, J. K., Neutralizing epitopes in the membrane-proximal external region of HIV-1 gp41 are influenced by the transmembrane domain and the plasma membrane. *J. Virol.* **2012,** *86* (6), 2930-2941.

(16) Apellaniz, B.; Rujas, E.; Serrano, S.; Morante, K.; Tsumoto, K.; Caaveiro, J. M.; Jimenez, M. A.; Nieva, J. L., The Atomic Structure of the HIV-1 gp41 Transmembrane Domain and Its Connection to the Immunogenic Membrane-proximal External Region. *J. Biol. Chem.* **2015,** *290* (21), 12999-13015.

(17) Lee, J. H.; Ozorowski, G.; Ward, A. B., Cryo-EM structure of a native, fully glycosylated, cleaved HIV-1 envelope trimer. *Science* **2016,** *351* (6277), 1043-1048.

(18) Dev, J.; Park, D.; Fu, Q.; Chen, J.; Ha, H. J.; Ghantous, F.; Herrmann, T.; Chang, W.; Liu, Z.; Frey, G.; Seaman, M. S.; Chen, B.; Chou, J. J., Structural basis for membrane anchoring of HIV-1 envelope spike. *Science* **2016,** *353* (6295), 172-175.

(19) Rujas, E.; Caaveiro, J. M.; Partida-Hanon, A.; Gulzar, N.; Morante, K.; Apellaniz, B.; Garcia-Porras, M.; Bruix, M.; Tsumoto, K.; Scott, J. K.; Jimenez, M. A.; Nieva, J. L., Structural basis for broad neutralization of HIV-1 through the molecular recognition of 10E8 helical epitope at the membrane interface. *Sci. Rep.* **2016,** *6*, 38177.

(20) Chiliveri, S. C.; Louis, J. M.; Ghirlando, R.; Baber, J. L.; Bax, A., Tilted, Uninterrupted, Monomeric HIV-1 gp41 Transmembrane Helix from Residual Dipolar Couplings. *J. Am. Chem. Soc.* **2018,** *140* (1), 34-37.

(21) Pinto, D.; Fenwick, C.; Caillat, C.; Silacci, C.; Guseva, S.; Dehez, F.; Chipot, C.; Barbieri, S.; Minola, A.; Jarrossay, D.; Tomaras, G. D.; Shen, X.; Riva, A.; Tarkowski, M.; Schwartz, O.; Bruel, T.; Dufloo, J.; Seaman, M. S.; Montefiori, D. C.; Lanzavecchia, A.; Corti, D.; Pantaleo, G.; Weissenhorn, W., Structural Basis for Broad HIV-1 Neutralization by the MPER-Specific Human Broadly Neutralizing Antibody LN01. *Cell Host Microbe* **2019,** *26* (5), 623-637 e628.

(22) Apellaniz, B.; Ivankin, A.; Nir, S.; Gidalevitz, D.; Nieva, J. L., Membrane-proximal external HIV-1 gp41 motif adapted for destabilizing the highly rigid viral envelope. *Biophys. J.* **2011,** *101* (10), 2426-2435.

(23) Apellaniz, B.; Nieva, J. L., Fusion-competent state induced by a C-terminal HIV-1 fusion peptide in cholesterol-rich membranes. *Biochim. Biophys. Acta* **2015,** *1848* (4), 1014-1022.

(24) Carravilla, P.; Cruz, A.; Martin-Ugarte, I.; Oar-Arteta, I. R.; Torralba, J.; Apellaniz, B.; Perez-Gil, J.; Requejo-Isidro, J.; Huarte, N.; Nieva, J. L., Effects of HIV-1 gp41-Derived Virucidal Peptides on Virus-like Lipid Membranes. *Biophys. J.* **2017,** *113* (6), 1301-1310.

(25) Apellaniz, B.; Rujas, E.; Carravilla, P.; Requejo-Isidro, J.; Huarte, N.; Domene, C.; Nieva, J. L., Cholesterol-Dependent Membrane Fusion Induced by the gp41 Membrane-Proximal External Region-Transmembrane Domain Connection Suggests a Mechanism for Broad HIV-1 Neutralization. *J. Virol.* **2014,** *88* (22), 13367-13377.

(26) Huang, J.; Ofek, G.; Laub, L.; Louder, M. K.; Doria-Rose, N. A.; Longo, N. S.; Imamichi, H.; Bailer, R. T.; Chakrabarti, B.; Sharma, S. K.; Alam, S. M.; Wang, T.; Yang, Y.; Zhang, B.; Migueles, S. A.; Wyatt, R.; Haynes, B. F.; Kwong, P. D.; Mascola, J. R.; Connors, M., Broad and potent neutralization of HIV-1 by a gp41-specific human antibody. *Nature* **2012,** *491* (7424), 406-412.

(27) Krebs, S. J.; Kwon, Y. D.; Schramm, C. A.; Law, W. H.; Donofrio, G.; Zhou, K. H.; Gift, S.; Dussupt, V.; Georgiev, I. S.; Schatzle, S.; McDaniel, J. R.; Lai, Y. T.; Sastry, M.; Zhang, B.; Jarosinski, M. C.; Ransier, A.; Chenine, A. L.; Asokan, M.; Bailer, R. T.; Bose, M.; Cagigi, A.; Cale, E. M.; Chuang, G. Y.; Darko, S.; Driscoll, J. I.; Druz, A.; Gorman, J.; Laboune, F.; Louder, M. K.; McKee, K.; Mendez, L.; Moody, M. A.; O'Sullivan, A. M.; Owen, C.; Peng, D.; Rawi, R.; Sanders-Buell, E.; Shen, C. H.; Shiakolas, A. R.; Stephens, T.; Tsybovsky, Y.; Tucker, C.; Verardi, R.; Wang, K.; Zhou, J.; Zhou, T.; Georgiou, G.; Alam, S. M.; Haynes, B. F.; Rolland, M.; Matyas, G. R.; Polonis, V. R.; McDermott, A. B.; Douek, D. C.; Shapiro, L.; Tovanabutra, S.; Michael, N. L.; Mascola, J. R.; Robb, M. L.; Kwong, P. D.; Doria-Rose, N. A., Longitudinal Analysis Reveals Early Development of Three MPER-Directed Neutralizing Antibody Lineages from an HIV-1-Infected Individual. *Immunity* **2019,** *50* (3), 677-691 e613.

(28) Jacob, R. A.; Moyo, T.; Schomaker, M.; Abrahams, F.; Grau Pujol, B.; Dorfman, J. R., Anti-V3/Glycan and Anti-MPER Neutralizing Antibodies, but Not Anti-V2/Glycan Site Antibodies, Are Strongly Associated with Greater Anti-HIV-1 Neutralization Breadth and Potency. *J. Virol.* **2015,** *89* (10), 5264-5275.

(29) Munro, J. B.; Gorman, J.; Ma, X.; Zhou, Z.; Arthos, J.; Burton, D. R.; Koff, W. C.; Courter, J. R.; Smith, A. B., 3rd; Kwong, P. D.; Blanchard, S. C.; Mothes, W., Conformational dynamics of single HIV-1 envelope trimers on the surface of native virions. *Science* **2014,** *346* (6210), 759-763.

(30) Lu, M.; Ma, X.; Castillo-Menendez, L. R.; Gorman, J.; Alsahafi, N.; Ermel, U.; Terry, D. S.; Chambers, M.; Peng, D.; Zhang, B.; Zhou, T.; Reichard, N.; Wang, K.; Grover, J. R.; Carman, B. P.; Gardner, M. R.; Nikic-Spiegel, I.; Sugawara, A.; Arthos, J.; Lemke, E. A.; Smith, A. B., 3rd; Farzan, M.; Abrams, C.; Munro, J. B.; McDermott, A. B.; Finzi, A.; Kwong, P. D.; Blanchard, S. C.; Sodroski, J. G.; Mothes, W., Associating HIV-1 envelope glycoprotein structures with states on the virus observed by smFRET. *Nature* **2019,** *568* (7752), 415-419.

(31) Stiegler, G.; Kunert, R.; Purtscher, M.; Wolbank, S.; Voglauer, R.; Steindl, F.; Katinger, H., A potent cross-clade neutralizing human monoclonal antibody against a novel epitope on gp41 of human immunodeficiency virus type 1. *AIDS. Res. Hum. Retroviruses* **2001,** *17* (18), 1757-1765.

(32) Cardoso, R. M.; Brunel, F. M.; Ferguson, S.; Zwick, M.; Burton, D. R.; Dawson, P. E.; Wilson, I. A., Structural basis of enhanced binding of extended and helically constrained peptide epitopes of the broadly neutralizing HIV-1 antibody 4E10. *J. Mol. Biol.* **2007,** *365* (5), 1533-1544.

(33) Williams, L. D.; Ofek, G.; Schatzle, S.; McDaniel, J. R.; Lu, X.; Nicely, N. I.; Wu, L.; Lougheed, C. S.; Bradley, T.; Louder, M. K.; McKee, K.; Bailer, R. T.; O'Dell, S.; Georgiev, I. S.; Seaman, M. S.; Parks, R. J.; Marshall, D. J.; Anasti, K.; Yang, G.; Nie, X.; Tumba, N. L.; Wiehe, K.; Wagh, K.; Korber, B.; Kepler, T. B.; Munir Alam, S.; Morris, L.; Kamanga, G.; Cohen, M. S.; Bonsignori, M.; Xia, S. M.; Montefiori, D. C.; Kelsoe, G.; Gao, F.; Mascola, J. R.; Moody, M. A.; Saunders, K. O.; Liao, H. X.; Tomaras, G. D.; Georgiou, G.; Haynes, B. F., Potent and broad HIV-neutralizing antibodies in memory B cells and plasma. *Sci. Immunol.* **2017,** *2* (7), 2200.

(34) Zhang, L.; Irimia, A.; He, L.; Landais, E.; Rantalainen, K.; Leaman, D. P.; Vollbrecht, T.; Stano, A.; Sands, D. I.; Kim, A. S.; Investigators, I. P. G.; Poignard, P.; Burton, D. R.; Murrell, B.; Ward, A. B.; Zhu, J.; Wilson, I. A.; Zwick, M. B., An MPER antibody neutralizes HIV-1 using germline features shared among donors. *Nat. Commun.* **2019,** *10* (1), 5389.

(35) Carravilla, P.; Chojnacki, J.; Rujas, E.; Insausti, S.; Largo, E.; Waithe, D.; Apellaniz, B.; Sicard, T.; Julien, J. P.; Eggeling, C.; Nieva, J. L., Molecular recognition of the native HIV-1 MPER revealed by STED microscopy of single virions. *Nat. Commun.* **2019,** *10* (1), 78.

(36) Irimia, A.; Sarkar, A.; Stanfield, R. L.; Wilson, I. A., Crystallographic Identification of Lipid as an Integral Component of the Epitope of HIV Broadly Neutralizing Antibody 4E10. *Immunity* **2016,** *44* (1), 21-31.

(37) Irimia, A.; Serra, A. M.; Sarkar, A.; Jacak, R.; Kalyuzhniy, O.; Sok, D.; Saye-Francisco, K. L.; Schiffner, T.; Tingle, R.; Kubitz, M.; Adachi, Y.; Stanfield, R. L.; Deller, M. C.; Burton, D. R.; Schief, W. R.; Wilson, I. A., Lipid interactions and angle of approach to the HIV-1 viral membrane of broadly neutralizing antibody 10E8: Insights for vaccine and therapeutic design. *PLoS. Pathog.* **2017,** *13* (2), e1006212.

(38) Oakes, V.; Torralba, J.; Rujas, E.; Nieva, J. L.; Domene, C.; Apellaniz, B., Exposure of the HIV-1 broadly neutralizing antibody 10E8 MPER epitope on the membrane surface by gp41 transmembrane domain scaffolds. *Biochim. Biophys. Acta Biomembr.* **2018,** *1860* (6), 1259-1271.

(39) Fu, Q.; Shaik, M. M.; Cai, Y.; Ghantous, F.; Piai, A.; Peng, H.; Rits-Volloch, S.; Liu, Z.; Harrison, S. C.; Seaman, M. S.; Chen, B.; Chou, J. J., Structure of the membrane proximal external region of HIV-1 envelope glycoprotein. *Proc. Natl. Acad. Sci. U. S. A.* **2018,** *115* (38), E8892-E8899.

(40) Yue, L.; Shang, L.; Hunter, E., Truncation of the Membrane-Spanning Domain of Human Immunodeficiency Virus Type 1 Envelope Glycoprotein Defines Elements Required for Fusion, Incorporation, and Infectivity. *J. Virol.* **2009,** *83* (22), 11588-11598.

(41) Rujas, E.; Leaman, D. P.; Insausti, S.; Ortigosa-Pascual, L.; Zhang, L.; Zwick, M. B.; Nieva, J. L., Functional Optimization of Broadly Neutralizing HIV-1 Antibody 10E8 by Promotion of Membrane Interactions. *J. Virol.* **2018,** *92* (8), e02249-17.

(42) Scherer, E. M.; Leaman, D. P.; Zwick, M. B.; McMichael, A. J.; Burton, D. R., Aromatic residues at the edge of the antibody combining site facilitate viral glycoprotein recognition through membrane interactions. *Proc. Natl. Acad. Sci. U. S. A.* **2010,** *107* (4), 1529-1534.

(43) Chojnacki, J.; Staudt, T.; Glass, B.; Bingen, P.; Engelhardt, J.; Anders, M.; Schneider, J.; Muller, B.; Hell, S. W.; Krausslich, H. G., Maturation-dependent HIV-1 surface protein redistribution revealed by fluorescence nanoscopy. *Science* **2012,** *338* (6106), 524-528.

(44) Grouleff, J.; Irudayam, S. J.; Skeby, K. K.; Schiott, B., The influence of cholesterol on membrane protein structure, function, and dynamics studied by molecular dynamics simulations. *Biochim. Biophys. Acta* **2015,** *1848* (9), 1783-1795.

(45) Legler, D. F.; Matti, C.; Laufer, J. M.; Jakobs, B. D.; Purvanov, V.; Uetz-von Allmen, E.; Thelen, M., Modulation of Chemokine Receptor Function by Cholesterol: New Prospects for Pharmacological Intervention. *Mol. Pharmacol.* **2017,** *91* (4), 331-338.

(46) Brügger, B.; Glass, B.; Haberkant, P.; Leibrecht, I.; Wieland, F. T.; Kräusslich, H. G., The HIV lipidome: a raft with an unusual composition. *Proc. Natl. Acad. Sci. U. S. A.* **2006,** *103* (8), 2641-2646.

(47) Huarte, N.; Carravilla, P.; Cruz, A.; Lorizate, M.; Nieto-Garai, J. A.; Krausslich, H. G.; Perez-Gil, J.; Requejo-Isidro, J.; Nieva, J. L., Functional organization of the HIV lipid envelope. *Sci. Rep.* **2016,** *6*, 34190.

(48) Apellaniz, B.; Nieva, J. L.; Schwille, P.; Garcia-Saez, A. J., All-or-none versus graded: single-vesicle analysis reveals lipid composition effects on membrane permeabilization. *Biophys. J.* **2010,** *99* (11), 3619-3628.

(49) McIntosh, T. J.; Simon, S. A., Bilayers as protein solvents: role of bilayer structure and elastic properties. *J. Gen. Physiol.* **2007,** *130* (2), 225-227.

(50) Epand, R. F.; Sayer, B. G.; Epand, R. M., The tryptophan-rich region of HIV gp41 and the promotion of cholesterol-rich domains. *Biochemistry* **2005,** *44* (14), 5525-5531.

(51) Lorent, J. H.; Diaz-Rohrer, B.; Lin, X.; Spring, K.; Gorfe, A. A.; Levental, K. R.; Levental, I., Structural determinants and functional consequences of protein affinity for membrane rafts. *Nat. Commun.* **2017,** *8* (1), 1219.

(52) Arrondo, J. L.; Goni, F. M., Structure and dynamics of membrane proteins as studied by infrared spectroscopy. *Prog. Biophys. Mol. Biol.* **1999,** *72* (4), 367-405.

(53) Lorent, J. H.; Levental, K. R.; Ganesan, L.; Rivera-Longsworth, G.; Sezgin, E.; Doktorova, M. D.; Lyman, E.; Levental, I., The mammalian plasma membrane is defined by transmembrane asymmetries in lipid unsaturation, leaflet packing, and protein shape. *bioRxiv* **2019**, 698837.

(54) Yuan, Z.; Zhang, F.; Davis, M. J.; Boden, M.; Teasdale, R. D., Predicting the solvent accessibility of transmembrane residues from protein sequence. *J. Proteome Res.* **2006,** *5* (5), 1063-1070.

(55) Shen, X.; Parks, R. J.; Montefiori, D. C.; Kirchherr, J. L.; Keele, B. F.; Decker, J. M.; Blattner, W. A.; Gao, F.; Weinhold, K. J.; Hicks, C. B.; Greenberg, M. L.; Hahn, B. H.; Shaw, G. M.; Haynes, B. F.; Tomaras, G. D., In vivo gp41 antibodies targeting the 2F5 monoclonal antibody epitope mediate human immunodeficiency virus type 1 neutralization breadth. *J. Virol.* **2009,** *83* (8), 3617-3625.

(56) Zhu, Z.; Qin, H. R.; Chen, W.; Zhao, Q.; Shen, X.; Schutte, R.; Wang, Y.; Ofek, G.; Streaker, E.; Prabakaran, P.; Fouda, G. G.; Liao, H. X.; Owens, J.; Louder, M.; Yang, Y.; Klaric, K. A.; Moody, M. A.; Mascola, J. R.; Scott, J. K.; Kwong, P. D.; Montefiori, D.; Haynes, B. F.; Tomaras, G. D.; Dimitrov, D. S., Cross-reactive HIV-1-neutralizing human monoclonal antibodies identified from a patient with 2F5-like antibodies. *J. Virol.* **2011,** *85* (21), 11401-11408.

(57) Li, Y.; Svehla, K.; Louder, M. K.; Wycuff, D.; Phogat, S.; Tang, M.; Migueles, S. A.; Wu, X.; Phogat, A.; Shaw, G. M.; Connors, M.; Hoxie, J.; Mascola, J. R.; Wyatt, R., Analysis of neutralization specificities in polyclonal sera derived from human immunodeficiency virus type 1-infected individuals. *J. Virol.* **2009,** *83* (2), 1045-1059.

(58) Gray, E. S.; Madiga, M. C.; Moore, P. L.; Mlisana, K.; Abdool Karim, S. S.; Binley, J. M.; Shaw, G. M.; Mascola, J. R.; Morris, L., Broad neutralization of human immunodeficiency virus type 1 mediated by plasma antibodies against the gp41 membrane proximal external region. *J. Virol.* **2009,** *83* (21), 11265-11274.

(59) Sather, D. N.; Stamatatos, L., Epitope specificities of broadly neutralizing plasmas from HIV-1 infected subjects. *Vaccine* **2010,** *28 Suppl 2*, B8-12.

(60) Stamatatos, L.; Morris, L.; Burton, D. R.; Mascola, J. R., Neutralizing antibodies generated during natural HIV-1 infection: good news for an HIV-1 vaccine? *Nat. Med.* **2009,** *15* (8), 866-870.

(61) Zhou, M.; Kostoula, I.; Brill, B.; Panou, E.; Sakarellos-Daitsiotis, M.; Dietrich, U., Prime boost vaccination approaches with different conjugates of a new HIV-1 gp41 epitope encompassing the membrane proximal external region induce neutralizing antibodies in mice. *Vaccine* **2012,** *30* (11), 1911-1916.

(62) Serrano, S.; Araujo, A.; Apellaniz, B.; Bryson, S.; Carravilla, P.; de la Arada, I.; Huarte, N.; Rujas, E.; Pai, E. F.; Arrondo, J. L.; Domene, C.; Jimenez, M. A.; Nieva, J. L., Structure and immunogenicity of a peptide vaccine, including the complete HIV-1 gp41 2F5 epitope: implications for antibody recognition mechanism and immunogen design. *J. Biol. Chem.* **2014,** *289* (10), 6565-6580.

(63) Salimi, H.; Johnson, J.; Flores, M. G.; Zhang, M. S.; O'Malley, Y.; Houtman, J. C.; Schlievert, P. M.; Haim, H., The lipid membrane of HIV-1 stabilizes the viral envelope glycoproteins and modulates their sensitivity to antibody neutralization. *J. Biol. Chem.* **2020,** *295* (2), 348-362.

(64) Alving, C. R.; Rao, M.; Steers, N. J.; Matyas, G. R.; Mayorov, A. V., Liposomes containing lipid A: an effective, safe, generic adjuvant system for synthetic vaccines. *Expert Rev. Vaccines* **2012,** *11* (6), 733-744.

(65) Carravilla, P.; Nieva, J. L.; Goñi, F. M.; Requejo-Isidro, J.; Huarte, N., Two-Photon Laurdan Studies of the Ternary Lipid Mixture DOPC:SM:Cholesterol Reveal a Single Liquid Phase at Sphingomyelin:Cholesterol Ratios Lower Than 1. *Langmuir* **2015,** *31* (9), 2808-2817.

(66) Buzon, V.; Natrajan, G.; Schibli, D.; Campelo, F.; Kozlov, M. M.; Weissenhorn, W., Crystal structure of HIV-1 gp41 including both fusion peptide and membrane proximal external regions. *PLoS Pathog.* **2010,** *6* (5), e1000880.

(67) Kawai, T.; Caaveiro, J. M. M.; Abe, R.; Katagiri, T.; Tsumoto, K., Catalytic activity of MsbA reconstituted in nanodisc particles is modulated by remote interactions with the bilayer. *FEBS Lett.* **2011,** *585* (22), 3533-3537.

(68) Galiani, S.; Waithe, D.; Reglinski, K.; Cruz-Zaragoza, L. D.; Garcia, E.; Clausen, M. P.; Schliebs, W.; Erdmann, R.; Eggeling, C., Super-resolution Microscopy Reveals Compartmentalization of Peroxisomal Membrane Proteins. *J. Biol. Chem.* **2016,** *291* (33), 16948-16962.

(69) Velasco-Olmo, A.; Ormaetxea Gisasola, J.; Martinez Galvez, J. M.; Vera Lillo, J.; Shnyrova, A. V., Combining patch-clamping and fluorescence microscopy for quantitative reconstitution of cellular membrane processes with Giant Suspended Bilayers. *Sci. Rep.* **2019,** *9* (1), 7255.

For Table of Contents Use Only:

Cholesterol constrains the antigenic configuration of the membrane-proximal neutralizing HIV-1 epitope

Johana Torralba, Igor de la Arada, Pablo Carravilla, Sara Insausti, Edurne Rujas, Eneko Largo, Christian Eggeling, José L. R. Arrondo, Beatriz Apellániz and José L. Nieva